ACS APPLIED MATERIALS & INTERFACES

Research Article

www.acsami.org

# Energy Dissipation Due to Interfacial Slip in Nanocomposites Reinforced with Aligned Carbon Nanotubes

Frank Gardea,[†] Bryan Glaz,[‡] Jaret Riddick,[‡] Dimitris C. Lagoudas,[†] and Mohammad Naraghi*[,†]

[†]Department of Aerospace Engineering, Texas A&M University, 3409 TAMU, College Station, Texas 77843-3409, United States

[‡]Vehicle Technology Directorate, U.S. Army Research Laboratory, Aberdeen Proving Ground, Maryland 21005-5066, United States

**ABSTRACT:** Interfacial slip mechanisms of strain energy dissipation and vibration damping of highly aligned carbon nanotube (CNT) reinforced polymer composites were studied through experimentation and complementary micromechanics modeling. Experimentally, we have developed CNT-polystyrene (PS) composites with a high degree of CNT alignment via a combination of twin-screw extrusion and hot-drawing. The aligned nanocomposites enabled a focused study of the interfacial slip mechanics associated with shear stress concentrations along the CNT-PS interface induced by the elastic mismatch between the filler and matrix. The variation of storage and loss modulus suggests the initiation of the interfacial slip occurs at axial strains as low as 0.028%, primarily due to shear stress concentration along the CNT-PS interface. Through micromechanics modeling and by matching the model with the experimental results at the onset of slip, the interfacial shear strength was evaluated. The model was then used to provide additional insight into the experimental observations by showing that the nonlinear variation of damping with dynamic strain can be attributed to slip-stick behavior. The dependence of the interfacial load-transfer reversibility on the dynamic strain history and characteristic time scale was experimentally investigated to demonstrate the relative contribution of van der Waals (vdW) interactions, mechanical interlocking, and covalent bonding to shear interactions.

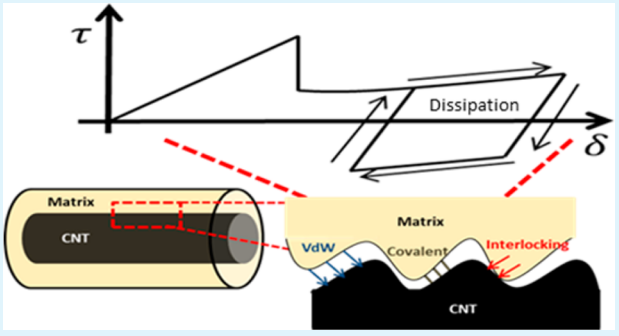


**KEYWORDS:** *interfacial slip, damping, slip-stick, mechanical interlocking*

## 1. INTRODUCTION

Structural integrity and safe operation of many structures, such as rotary wings[1] and radar antennas,[2] relies on their ability to damp vibrations and dynamic instabilities. Undesired vibrations may severely compromise structural performance by inducing fatigue damages and/or high strains. In addition, in cases such as rotorcrafts, rotary-wing damping and stability can potentially enable advanced concepts that are currently infeasible, with potential benefits including damperless bearingless rotors, soft-in-plane tiltrotors, and reduced operating and maintenance costs.[1,3] Traditional approaches to suppress vibration in structures often includes the incorporation of auxiliary dampers (i.e., polymer tapes[4]) which leads to increased weight and footprint of the component. A potential alternative to auxiliary dampers is to take advantage of the inherent damping capability in structural materials, such as polymer composites, which is the focus of this study. Significant attention and research interest has focused on the use of polymers because of their low density and high processability.[5−7] One downfall, however, is the limited inherent damping capability of polymers. In addition, typically, a trade-off between loss modulus and stiffness is inevitable.[8] Although polymers show the largest damping capability near the glass-transition temperature, the polymer stiffness (e.g., storage modulus) is often significantly reduced near that temperature.[9]

One approach to improve the energy dissipation in polymers, without compromising effective stiffness and strength, is embedding nanoparticles into polymers. The large surface to volume ratio of carbon nanotubes (CNTs) and carbon nanofibers (CNFs), rooted in their submicrometer diameter, relative to many other types of reinforcements, such as carbon fibers, offers a great opportunity to dissipate energy and damp vibrations in composites via interfacial sliding. In addition, because of their remarkable intrinsic properties, such as high strength and modulus, these graphitic nanoparticles can effectively enhance the strength and stiffness of the composite materials.[10−12]

Even though nanoscale reinforcements have the potential to improve the effective composite properties, this ability is highly dependent on the mechanics of the reinforcement-polymer interface. In general, enhancing the strength and stiffness of a polymer by adding nanoscale fillers, e.g., CNTs, requires efficient load transfer between the filler and matrix, with limited or no sliding. On the other hand, relative sliding of the filler and matrix along their interface can lead to mechanical energy dissipation because of frictional sliding. This mode of energy dissipation is augmented by the large surface to volume ratio of

Received: February 17, 2015
Accepted: April 23, 2015
Published: April 23, 2015

ACS Publications © 2015 American Chemical Society



DOI: 10.1021/acsami.5b01459
ACS Appl. Mater. Interfaces 2015, 7, 9725−9735

the nanoscale reinforcements. This mechanism would be in addition to any existing inherent structural damping capability of the matrix.

Recent studies have alluded to the potential of nanoscale fillers to augment damping in materials. For example, Suhr and Karatkar studied the CNT slip mechanism in a randomly oriented CNT/polycarbonate system. They observed a significant increase (4−5 times) in loss modulus with the addition of 1.5 wt % single-walled CNTs.[13] However, random alignment of CNTs introduces complicated stress fields within the matrix, leading to energy dissipation mechanisms, such as matrix tearing and plasticity, in addition to CNT sliding. Therefore, quantitatively, it is not clear how much of the improvement in loss modulus is due to interfacial sliding in the nanocomposite.

Ogasawara et al. showed a hysteretic behavior in multiwalled CNT/PEEK composites under both tensile and compressive loading, whereas the neat PEEK polymer shows no hysteretic effect at strains below 1.5%. They attribute this behavior to slippage of the CNT-PEEK interface resulting from weak interaction.[14] Studies by Gong et al. pointed to an initial increase in loss modulus of polycarbonate/MWCNT composites with increasing strain.[9] At sufficiently large strains, once a maximum value in loss modulus was reached, the loss modulus decreased with strain. They attributed the decrease in loss modulus with increasing strain to a decrease in free volume and fractional free volume, resulting from the order arrangement in the chain segments.

Analytical models have also been developed to explain damping in composite materials. Cox developed a shear lag model in which a single fiber surrounded by matrix in the form of concentric cylinders are considered.[15] This model considers perfect bonding between the fiber and matrix. According to this model, the enhanced damping of a discontinuous fiber-reinforced matrix, compared to the neat matrix, is mainly due to a viscoelastic energy dissipation mechanism associated with stress concentration at the fiber ends, induced by elastic mismatch between the filler and matrix. Ang et al. extended the shear lag model to CNTs with a nonbonded interface.[16] This model points to the importance of interfacial factors such as mechanical interlocking, van der Waals interactions, thermal residual stress, and Poisson's contraction on the stress transfer and energy dissipation at the CNT/polymer interface. Esteva et al. concluded through micromechanics modeling that interface weakening significantly influences nanocomposite properties only for high SWCNT volume fractions (>0.6%).[17] Glaz et al., developed a micromechanics model to study the effect of interfacial slippage on damping and energy dissipation in nanocomposites.[1] According to their model, frictional forces at the interface increase the loss modulus with dynamic strain. If the shear stress at the interface is below a critical value, the nanoparticle and matrix remain bonded. As the shear stress increases to a critical value (critical shear stress), the particle will debond from the matrix (slip).[13,18] During the slip process, energy is dissipated through heat caused by the frictional sliding at the interface.

The current work aims at investigating the potential of CNT fillers in enhancing the damping properties of polymer matrix composites. The CNTs in our nanocomposites were mainly oriented along the loading direction via hot-drawing (above the glass-transition temperature of the matrix), in order to suppress energy dissipation modes such as matrix tearing, thus targeting the study on the effect of interfacial sliding to overall damping. We studied damping via dynamic mechanical analysis, and the ratio of the loss to storage modulus was used to compare the damping performance of the neat polymer and the CNT reinforced polymer. Through exploring the dependence of damping on frequency of loading and dynamic strain history, we have shed light on the nature of the CNT−matrix interactions.

## EXPERIMENTAL SECTION

The sources for energy dissipation in aligned composite materials, shown in Figure 1, may be divided into the following:[19] (1) far field viscoelastic damping in the matrix, (2) damping due to stress concentration at the matrix region surrounding the filler, (3) damping due to interfacial slip, (4) inherent damping in the filler (however, it is assumed the CNT remains elastic,[20] and thus the latter contribution is negligible). By aligning the CNTs in the loading direction, it is possible to suppress damping mechanisms such as matrix shearing, and thus focus our efforts on identifying the role of interfacial slip on overall damping.

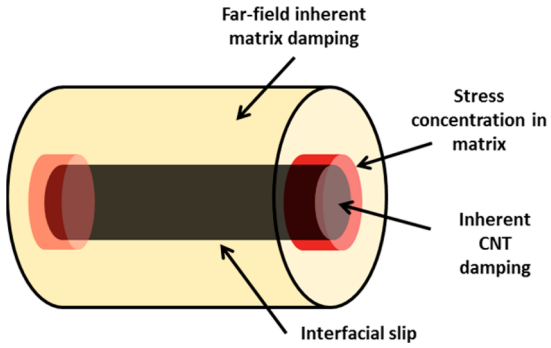


**Figure 1.** Schematic showing the sources of dissipation in an aligned CNT composite.

The steps of debonding and damping are assumed to follow that shown in Figure 2. In the initial configuration, step 1, CNT and matrix interact with each other via a combination of covalent bonds, mechanical interlocking, and van der Waals interactions. The interface of the CNT and matrix remains intact upon the application of static or dynamic load, as shown in step 2, until a critical shear stress for debonding is reached, at which the initial bonds and interactions are broken (step 3). Broken covalent bonds are nonreversible, whereas mechanical interlocking and van der Waals (vdW) are reversible. This leads to the "stick" mechanism. Upon dynamic loading, the mechanical interlocking and vdW interactions that were reformed are once again broken and slip occurs at the interface (during step 4 to step 5, dissipation of energy occurs). These interactions are again reformed upon reverse loading. The critical strain to initiate slippage is again reached at step 6, followed by slippage at the interface and further dissipation of energy (step 6 to step 7). Upon reaching step 7, the mechanical and vdW interactions are reformed. The cycle is then repeated.

**2.1. Processing.** Multiwalled carbon nanotubes with an outer diameter of 30−50 nm and length of 10−20 $\mu$m were purchased from Cheap Tubes Inc. and were used as is with no surface functionalization. Polystyrene (PS), with a density of 1.04 g/cm$^3$, was purchased from Sigma-Aldrich Co. and used as the matrix material. The fabrication of composites consisted of mixing a 1 wt % concentration of pristine CNTs in PS via a twin-screw microextruder. To this end, the polymer was first heated to 150 °C (above $T_g$ of ∼100 °C) inside the extruder. The dry CNTs were then poured into the extruder. Mixing was carried out at 100 rpm and 150 °C for 30 min. The CNT/polystyrene mixture was then extruded through a 5 mm × 0.5 mm dye at 25 rpm. As the polymer mixture was being extruded, mechanical stretching (hot-drawing) was performed. The aim of mechanical stretching was to induce CNT alignment within the matrix.


DOI: 10.1021/acsami.5b01459
ACS Appl. Mater. Interfaces 2015, 7, 9725−9735

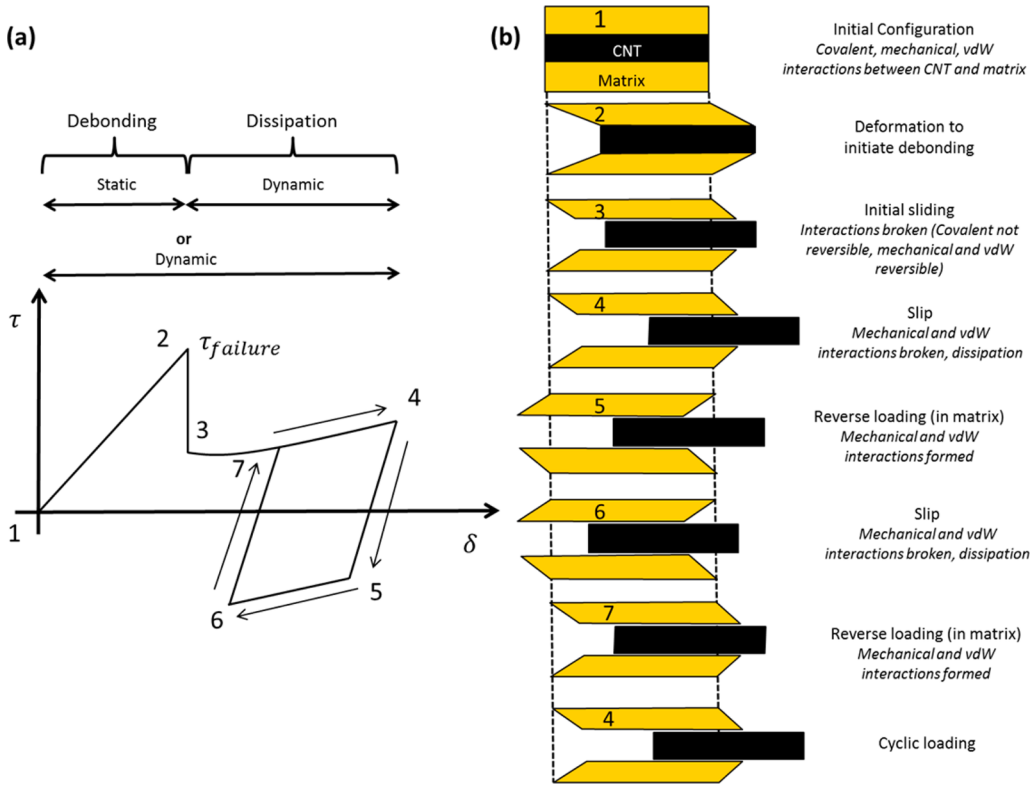


**Figure 2.** (a) Schematic showing steps of debonding and damping as a function of relative displacement $\delta$. (b) Schematic representation of CNT slippage during loading. Numbers correspond to critical steps during the loading cycle as mentioned in the text. Dissipation of energy occurs at steps 4 and 6.

A stretch ratio of 8 was achieved, estimated as the ratio of the cross section area of the unstretched to stretched samples, assuming volume conservation. Neat polymer samples were fabricated for comparison (stretch ratio was kept the same between the neat and reinforced samples). High-resolution scanning electron microscope (SEM) images of the cross-sections of the composite, with planes of cut being parallel and perpendicular to the stretching direction, were used to study the effectiveness of hot-drawing in inducing alignment of CNTs. SEM images were obtained using a JEOL JSM-7500F FE-SEM. In addition, polarized Raman spectroscopy was performed to study the alignment of CNTs using a Horiba Jobin-Yvon LabRam Raman Confocal Microscope with a 785 nm laser. The polarized incident laser was rotated in the direction parallel and perpendicular to the stretching direction using a half-wave plate. The ratio of the D-band peak, corresponding to disorder in the CNT crystalline symmetry, between the parallel and perpendicular directions was used as a measure of CNT alignment.

**2.2. Mechanical Characterization.** Dynamic mechanical analysis (DMA) was performed on CNT reinforced polystyrene nanocomposites and neat polystyrene samples at various dynamic strain amplitudes using a TA Instruments RSAIII DMA. All dynamic testing was performed in the direction of CNT alignment. The tests consisted of a dynamic strain sweep, in which the amplitude was varied from 0.01 to 1%. Within this range, no sample buckling was observed during the compressive half-cycles. The frequency was set to 1.0 Hz. From an application perspective, frequencies for this study were ≤1 Hz, which is in the order of magnitude required for rotor aeromechanical stability.[1] Due to the low frequency loading, the study remains quasi-static with in-phase relative motion of the filler and matrix when responding to the applied strain. During this test the offset strain was set to zero. Accumulation of damage was also studied by measuring the repeatability of damping at varying dynamic strains. In order to identify the frequency dependence on the interfacial sliding and damping, tests were performed at 0.1 and 1 Hz. Through these experiments, the nature of shear interactions between the matrix and the filler was identified.

## 3. MODELING

To interpret the experimentally measured damping in CNT-reinforced nanocomposites, we used the model developed by Glaz et al. that considers interfacial slip as the sole source of damping in addition to the inherent damping of the matrix.[1] The interfacial shear stress in the model by Glaz et al. is taken from the continuum model by Cox[15] developed originally for discontinuous fiber reinforcements prior to fiber-matrix slippage. In the postslip regime, the frictional energy dissipation is assumed to be proportional to the interfacial shear force, $f(\varepsilon_{xx})$, as shown in eq 1 where $r_{NI}$ is the radius of the nanoinclusion, $\tau_c$ is the critical interfacial shear stress, and $l'$ is the interface length over which interfacial slip occurs.

$$f(\varepsilon_{xx}) = 2\pi r_{NI}\tau_c \frac{l'(\varepsilon_{xx})}{2} \quad (1)$$

The critical shear stress to initiate slip is calculated by setting $x = 0$ and $\tau(x) = \tau_c$ in eq 2[15] where $d_{NI}$ is the diameter of the inclusion, $E_{NI}$ is the longitudinal modulus of the inclusion, $\varepsilon_{xx}$ is the applied strain. The value of $\beta$ is obtained from eq 3, where $G_m$ is the matrix shear modulus, $A_{NI}$ is the area of the inclusion, $v_f$ is the volume fraction, and $l$ is the inclusion length. The model assumes once the slip is initiated, the shear stress remains constant along the slipped zone, equal to the critical shear stress, because the matrix can transfer no more load to the CNT over this zone.[1]


DOI: 10.1021/acsami.5b01459
ACS Appl. Mater. Interfaces 2015, 7, 9725−9735

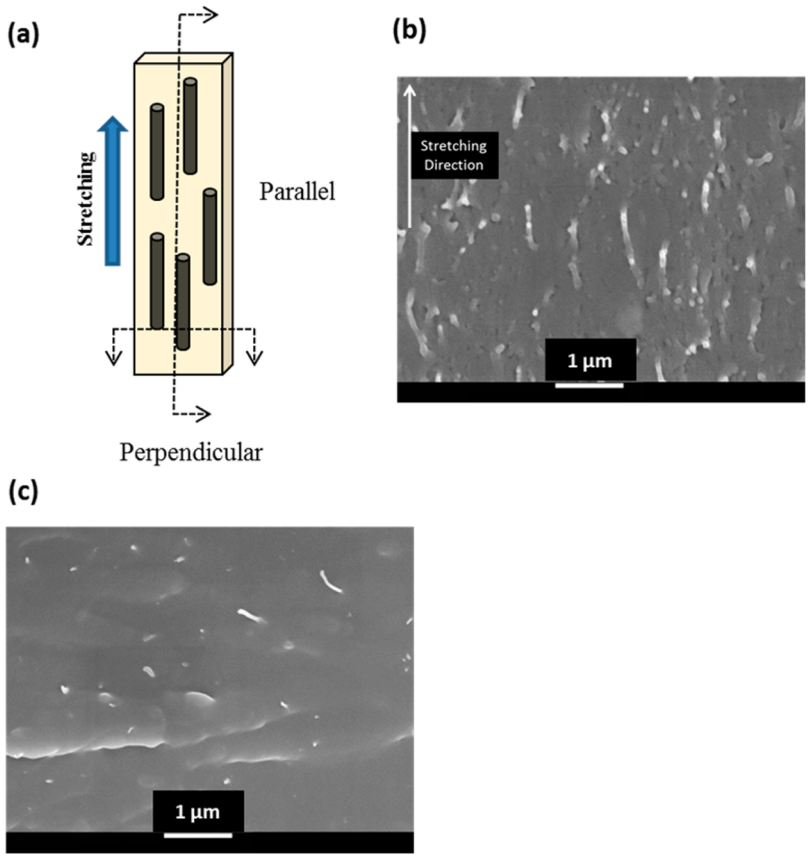


**Figure 3.** (a) Schematic of fractured surfaces perpendicular and parallel to stretching direction. (b) SEM image of fractured surface parallel to stretching direction showing alignment of CNTs in the direction of stretching. (c) SEM image of fractured surface perpendicular to the stretching direction showing the cross-section of fractured CNTs.

$$\tau(x) = \frac{d_{NI}E_{NI}\varepsilon_{xx}\beta}{4}\left[\frac{\sinh(\beta(l/2 - x))}{\cosh(\beta l/2)}\right] \quad (2)$$

$$\beta^2 = \frac{2\pi G_m}{A_{NI}E_{NI}\ln(1/\sqrt{v_f})} \quad (3)$$

Furthermore, the critical applied strain at which interfacial slip initiates, $\varepsilon'$, is calculated in eq 4.

$$\varepsilon' = \frac{4\tau_c}{d_{NI}E_{NI}\beta\tanh(\beta l/2)} \quad (4)$$

Also, the length over which slip occurs is obtained from eq 5.

$$l' = l - \frac{2}{\beta}\sin h^{-1}\left(\frac{4\tau_c\cosh(\beta l/2)}{d_{NI}E_{NI}\varepsilon_{xx}\beta}\right) \quad (5)$$

Once interfacial slip initiates, the stiffness contribution from the nanoinclusion, $K_{NI}$, decreases and can be estimated by an appropriate decay function or through the experiments. The effective composite stiffness, $\bar{K}$, post slip is shown in eq 6. $K_M$ is the matrix stiffness, $K_{NI,0}$ is the initial inclusion stiffness, $\varepsilon_1 = \max(\varepsilon',\varepsilon_0)$, $\varepsilon_{min} = \min(\varepsilon',\varepsilon_0)$ and $(\varepsilon_{max} = \varepsilon_0 + \varepsilon_\omega)$ where $\varepsilon_0$ is the offset strain and $\varepsilon_\omega$ is the dynamic strain.

$$\bar{K} = \frac{(K_M + K_{NI,0})(\varepsilon' - \varepsilon_{min}) + \int_{\varepsilon_1}^{\varepsilon_{max}}(K_M + K_{NI}(\varepsilon_{xx}))d\varepsilon_{xx}}{\varepsilon_{max} - \varepsilon_{min}} \quad (6)$$

From the effective stiffness, the corresponding storage modulus, $E_{storage}$, can be calculated from eq 7, whereas the maximum strain energy, $2\pi U_0$, and the dissipated energy, $\delta U$, can be calculated from eqs 8 and 9, respectively.

$$E_{storage} = \frac{\bar{K}l/2}{A_{RVE}} \quad (7)$$

$$2\pi U_0 = \frac{\pi}{4}\bar{K}(\varepsilon_\omega l)^2 \quad (8)$$

$$\delta U = 2\int_{\varepsilon_1}^{\varepsilon_{max}} f(\varepsilon_{xx})\frac{l'(\varepsilon_{xx})}{2}d\varepsilon_{xx} \quad (9)$$

Therefore, the loss factor, $\eta = \tan\delta$, is obtained from eq 10 and the loss modulus, $E_{loss}$, calculated from eq 11.

$$\eta = \frac{\delta U}{2\pi U_0} \quad (10)$$

$$E_{loss} = \eta E_{storage} \quad (11)$$

## 4. RESULTS AND DISCUSSION

### 4.1. Alignment of CNTs in the Matrix via Hot-Drawing.

The samples tested were fabricated using the method described in Section 2. Alignment of CNTs was qualitatively studied by fracturing the sample in the directions perpendicular and along the stretching direction, and observing CNT directions via SEM. The two directions are schematically shown in Figure 3a. SEM images of the fracture surface parallel to the stretching


DOI: 10.1021/acsami.5b01459
ACS Appl. Mater. Interfaces 2015, 7, 9725−9735

direction (Figure 3b) contains many cases of CNTs laid parallel to that direction, qualitatively verifying the preferred alignment of CNTs in the stretching direction during sample processing. The arrangement of CNTs on the surface parallel to the stretching direction is in contrast to the surface that is perpendicular to the stretching direction (Figure 3c), on which mostly broken CNT and holes (evidence of pull out) are observed.

Further evidence in support of the alignment of CNTs in the direction of hot-drawing was obtained via Raman spectroscopy. The basics of detecting CNT alignment via Raman spectroscopy relies on prior studies demonstrating that the intensity of the G-band and D-band in multiwalled carbon nanotubes depend on the laser polarization direction.[21] Specifically, the disorder peak (D-band) shows a correlation with the angle between the polarization of the incident laser and the CNT axis, with maximum scattering intensity along the CNT axis direction.[22] The G-band was not used as the metric for alignment because of the polystyrene matrix containing a peak in the same wavelength as the G-band (1520−1600 $cm^{-1}$). To detect CNT alignment, hot-drawn samples were subjected to polarized Raman spectroscopy with the polarization of the incident laser being parallel (0°) and perpendicular (90°) to the stretching direction. The ratio of the intensities of the D-band peak between the two polarization directions was used as a measure of the CNT alignment. This ratio was also measured on nanocomposites with randomly oriented CNTs (no hot-drawing) as the benchmark. The results are shown in Figure 4. The ratio of the parallel to perpendicular D-band (1310 $cm^{-1}$) intensity peak for the aligned CNT specimen was 1.36, whereas the random CNT specimen showed a considerably lower ratio of 1.15. This result shows that the CNT orientation coincides with the stretching direction, verifying the CNTs are aligned in the stretching direction.

**4.2. Energy Dissipation through Interfacial Slippage.** The dependence of the storage modulus on dynamic strain of CNT reinforced polystyrene nanocomposites and neat polystyrene are shown in Figure 5. As shown in the figure, at dynamic strains (<0.1%) the storage modulus of the 1 wt % composite is slightly higher than the neat PS. This is consistent with a rule of mixtures (RoM) prediction, obtained for the case of highly aligned and high aspect ratio CNTs, with the stiffness of their outer shell being in the range of 702 GPa−1.17 TPa, as presented in the Appendix.

Moreover, the storage modulus remains nearly independent of dynamic strain amplitude until a critical value of 0.028% is reached, after which, the storage modulus decreases with dynamic strain amplitude. The loss in storage modulus and deviation from RoM calculation is likely due to a loss in interfacial load transfer. In other words, the decrease in storage modulus with dynamic strain suggests that slippage initiates at this critical strain. SEM images of the fracture surfaces of CNT-PS composites, with many instances of CNT pull out and holes within the matrix from which CNTs have likely pulled out (Figure 6), provides further evidence in support of interfacial slippage, facilitated by sufficiently weak interfaces.

This result points to the significance of CNT−polymer interface engineering in enhancing the mechanics of polymer composites, as with no surface functionalization (the case studied here), interfacial slip can initiate at very low strains (as low as 0.028%), suppressing or eliminating the reinforcing effect of CNTs. Therefore, assessment of the contribution of CNTs to composite stiffness should also be carried out at

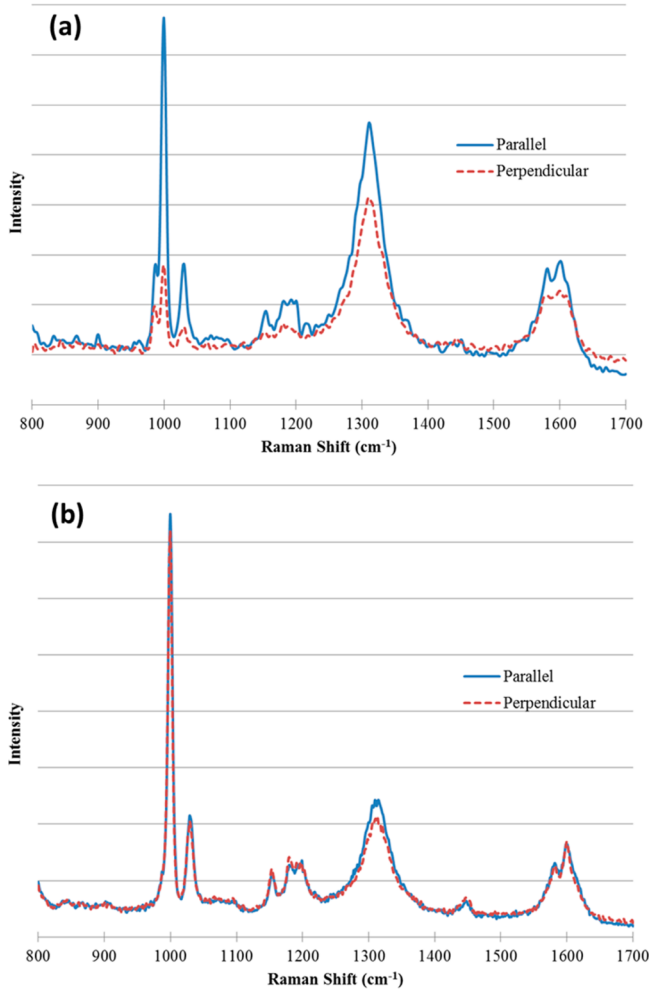


**Figure 4.** Polarized Raman spectra at 0° (parallel) and 90° (perpendicular) to the stretching direction for (a) aligned CNT/polystyrene composite and (b) randomly oriented CNT/polystyrene composite.

sufficiently low strains (below the critical sliding) and by considering the state of interfacial damage. For instance, in the case of pristine CNTs in PS which was studied here, where the interfacial slip occurs at 0.028%, the storage modulus at strains as low as 0.1% drops to the value of neat matrix, whereas at sufficiently lower strains, it follows the RoM predictions, as discussed earlier. This factor, interfacial slip promoted by the elastic mismatch between CNTs and polymer and weak interfaces, next to other microstructural defects, such as CNT agglomeration (not observed in this study) commonly referred to in the literature, should be considered in the assessment of mechanics and design of CNT composites.

Further evidence in support of the initiation of interfacial sliding at the critical strain of 0.028% is obtained by considering the variations of the damping capabilities of CNT-PS composites. As shown in Figure 7a, the tan $\delta$ of CNT-PS composite varies in a nonlinear fashion with dynamic strain amplitude in contrast to the nearly linear variations of the neat polymer. More specifically, at low strains, below the critical strain value, the measured tan $\delta$ is the same for both systems and nearly independent of the dynamic strain (Figures 5 and 7). However, when the critical dynamic strain is reached, the damping and energy dissipation in CNT-PS composite is markedly enhanced and increases with the dynamic strain.


DOI: 10.1021/acsami.5b01459
ACS Appl. Mater. Interfaces 2015, 7, 9725−9735

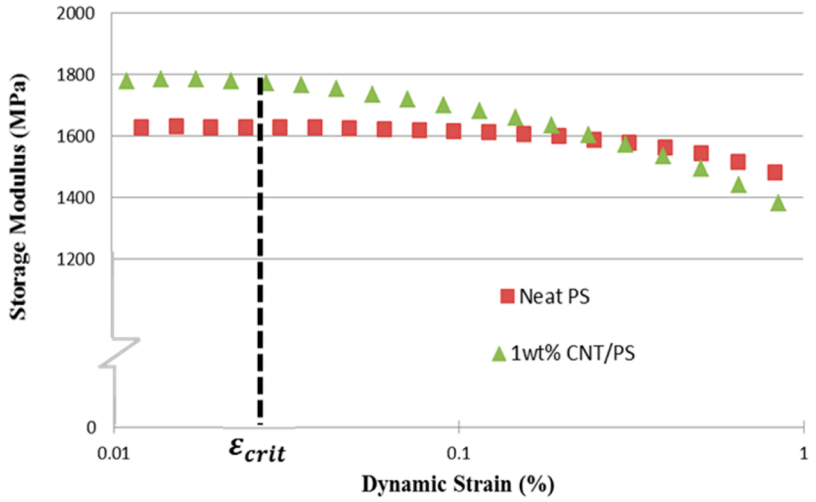


**Figure 5.** Experimental results of storage modulus as a function of dynamic strain for neat polystyrene (PS) and 1 wt % aligned CNT/PS composite. Offset strain = 0.0%, frequency = 1 Hz.

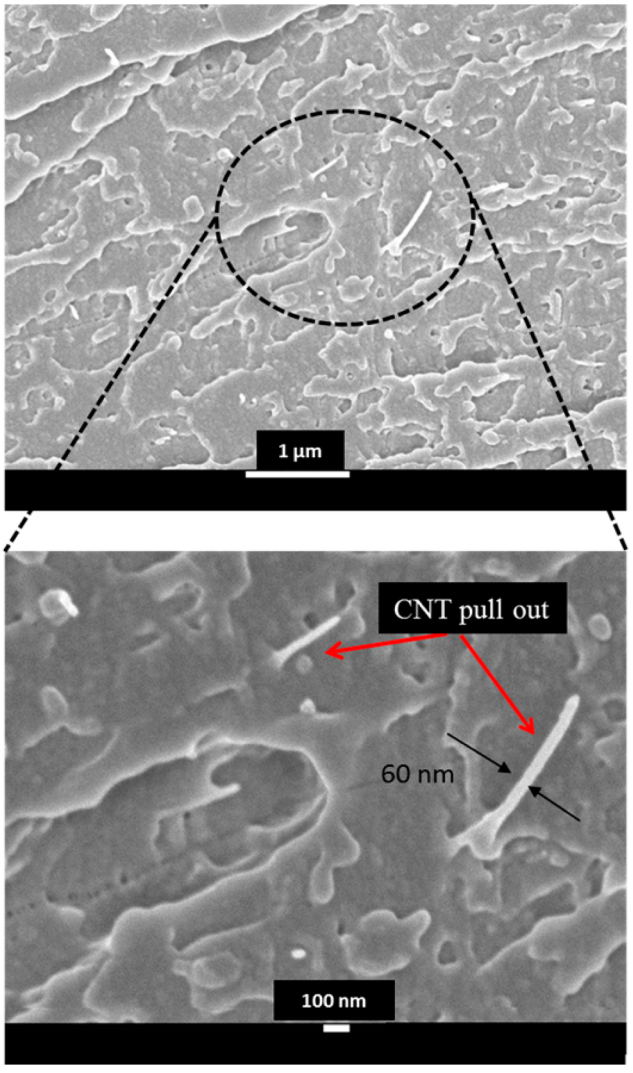


**Figure 6.** SEM images of fractured surface showing CNT pull out.

Assuming that the CNTs themselves remain elastic at these low values of average stress (below 100 MPa, compared to the strength of CNTs of several to tens of GPa),[20] the additional source of energy dissipation (in excess of inherent energy dissipation in matrix) could have stemmed from[19] (i) dissipation at the interface through slip or (ii) dissipation by the matrix because of stress concentrations at the CNT ends,[23−25] as schematically shown in Figure 1. The latter mechanism is considered to be one of the main damping mechanisms in microfiber reinforced composites.[26,27] Because the initiation strain of the additional energy dissipation mechanism coincides with dynamic strain at which material degradation starts (loss in storage modulus as shown in Figure 5), the former mechanism is considered to be the dominant factor contributing to the additional energy dissipation in CNT-PS composites. It is to be noted that by aligning the CNTs in the loading direction, other energy dissipation mechanisms, such as matrix plasticity and tearing, are suppressed.

**4.3. Micromechanics Modeling of Interfacial Dissipation through CNT Slippage.** To better illustrate the role of interfacial slip, we implemented a micromechanics model by Glaz et al.,[1] which only accounts for energy dissipation of aligned matrix inclusions from slippage. As shown experimentally before, the additional energy dissipation is dominantly caused by friction between CNT and matrix during slippage. The experimental results shown in Figure 8 correspond to only the contribution to damping resulting from the presence of the CNT, i.e., the polymer tan $\delta$ was subtracted from the composite tan $\delta$. The model parameters used are shown in Table 1. The density of both the CNTs and the matrix were obtained from the manufacturer specifications. In addition, the diameter of the CNT was taken as the average value of the diameter range given by the manufacturer. The elastic modulus of the matrix was taken from the DMA results of the neat polymer at the lowest tested strain. Using the onset strain, 0.028%, at which the CNT composite experimental tan $\delta$ deviates from that of the neat polymer, the interfacial shear strength was calculated using eq 4. The values obtained for the interfacial shear strength, $\tau_c$, range from 0.443 to 0.523 MPa for the cases studied. These results are comparable to that reported in literature for CNT composites.[28] The calculated value of $\tau_c$ varies for each case because of the varied length of the CNT or the modulus of the CNT, according to eq 4; however, the critical strain to initiate slip is obtained from the experiment and kept constant.


DOI: 10.1021/acsami.5b01459
ACS Appl. Mater. Interfaces 2015, 7, 9725−9735

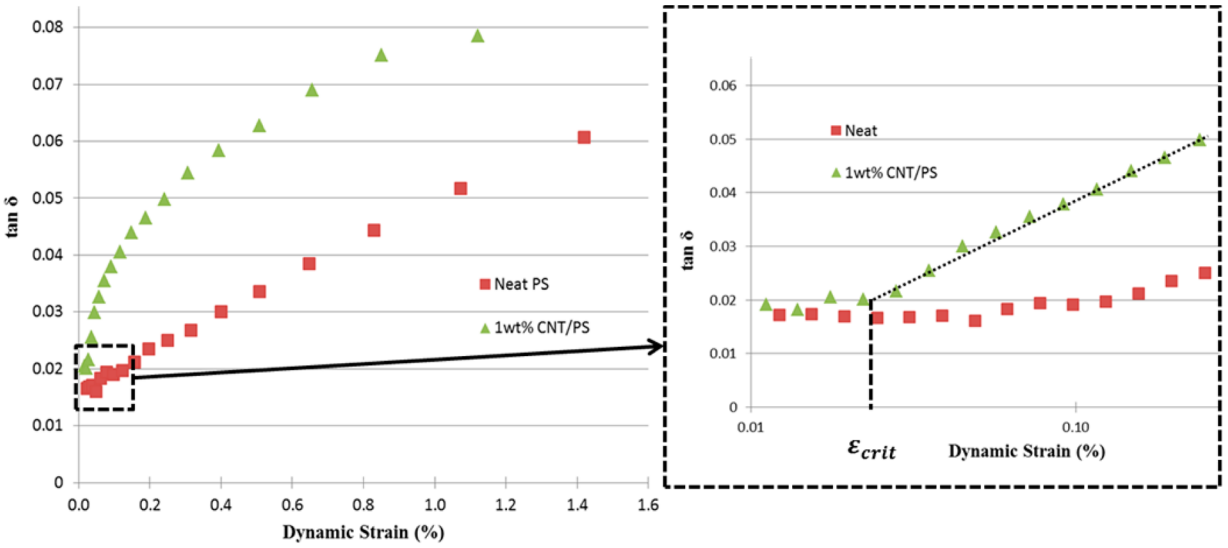


**Figure 7.** Experimental results of tan $\delta$ as a function of dynamic strain for neat polystyrene (PS) and 1 wt % aligned CNT/PS composite. Offset strain = 0.0%, frequency = 1 Hz.

**Table 1. Input Data for Micromechanics Model**

| | |
|---|---|
| matrix elastic modulus | 1.6 GPa |
| critical strain (slip initiation) | 0.028% |
| CNT concentration | 1 wt % |
| matrix density | 1.04 g/cm$^3$ |
| CNT density | 2.1 g/cm$^3$ |
| CNT diameter | 40 nm |
| frequency | 1 Hz |

The result in Figure 8a shows that the additional damping is highly dependent on the aspect ratio of the filler. The best approximation to the experimental result consists of fillers with an aspect ratio between 10 and 50, CNT length of 400 nm and 2 $\mu$m, respectively, shorter than the length reported by the manufacturer (10−20 $\mu$m). One explanation for this result would be that the CNTs were possibly cut during the fabrication process, resulting in much shorter CNTs. This is verified by the SEM images obtained, Figure 6, showing CNT pull-out. Assuming that only half of the length of the CNT on average is pulled out of the matrix, the images show an aspect ratio of about 15, consistent with the modeling results. The comparison of the model to the experimental results suggests that there exists additional energy dissipation mechanisms, such as accentuated energy dissipation in the matrix at the two ends of each CNT because of stress concentration.[26,27] The fact that this additional energy dissipation—the difference between the model prediction and experiment—is the largest at the lowest dynamic strain (onset of sliding), and decreases with dynamic strain amplitude (as the slippage zone spreads along the CNT) further supports this hypothesis.

**4.4. Further Insight into the Nature of Shear Interfacial Forces.** The interfacial shear strength is due to a combination of mechanical interlocking (compressive) and adhesion (attractive) interactions. The former reflects the tendency of the matrix and filler to prevent interpenetration during sliding, and thus it depends on surface topography and the mechanics of each phase. Mechanical interlocking arises from the surface roughness present on the CNT. The polymer conforms to this surface topography during the fabrication process. Upon relative displacement between the polymer and CNT, the roughness will give rise to a frictional component for dissipation. On the other hand, adhesion is a function of chemistry of the two surfaces, and may stem from a combination of vdW interactions and/or covalent bonds. Therefore, three main mechanisms are responsible for load transfer from a matrix to a filler: mechanical interlocking, chemical bonding, and van der Waals interactions,[29] as schematically shown in Figure 9.

Experiments were designed to shed light on the relative significance of these three types of interactions on the interfacial energy dissipation and damping in CNT-PS composites. First, we considered the ability of the vdW interactions and mechanical interlocking to reform upon initial rupture, for instance during interfacial sliding, which distinguishes them from covalent bonds. As shown in Figure 10, the dissipation in the CNT-PS composite samples as a function of the dynamic strain amplitude is nearly independent of the prior history of dynamic loading in the material. For instance, in the first cycle of loading, the material demonstrates additional energy dissipation mechanisms, relative to neat PS, at a critical strain of 0.028%, suggesting an initiation of interfacial slippage. However, at the beginning of the second cycle, when the dynamic strain is reduced to below the critical strain, the energy dissipation reduces to the levels of the neat PS, indicating the reformation of the initial interfacial interactions which prevent interfacial sliding. Therefore, the observed strain energy dissipation is mostly caused by the reformable interfacial interactions, vdW interactions and/or mechanical interlocking, and covalent bonds do not significantly contribute to the damping. This result is consistent with studies performed on the interactions between CNTs and polystyrene, which show that van der Waals and mechanical interlocking are the dominating interfacial interactions,[30,31] and no covalent bonding has formed, for instance as a result of chain scissor and repolymerization at high temperatures during extrusion.

Further insight into the relative contribution of mechanical interlocking and vdW interactions on interfacial slip was obtained via exploring the frequency dependence of interfacial shear strength, as shown in Figure 11. We considered two frequencies: 0.1 and 1.0 Hz. The results show that the critical dynamic strain amplitude for slip initiation increases as the


DOI: 10.1021/acsami.5b01459
ACS Appl. Mater. Interfaces 2015, 7, 9725−9735

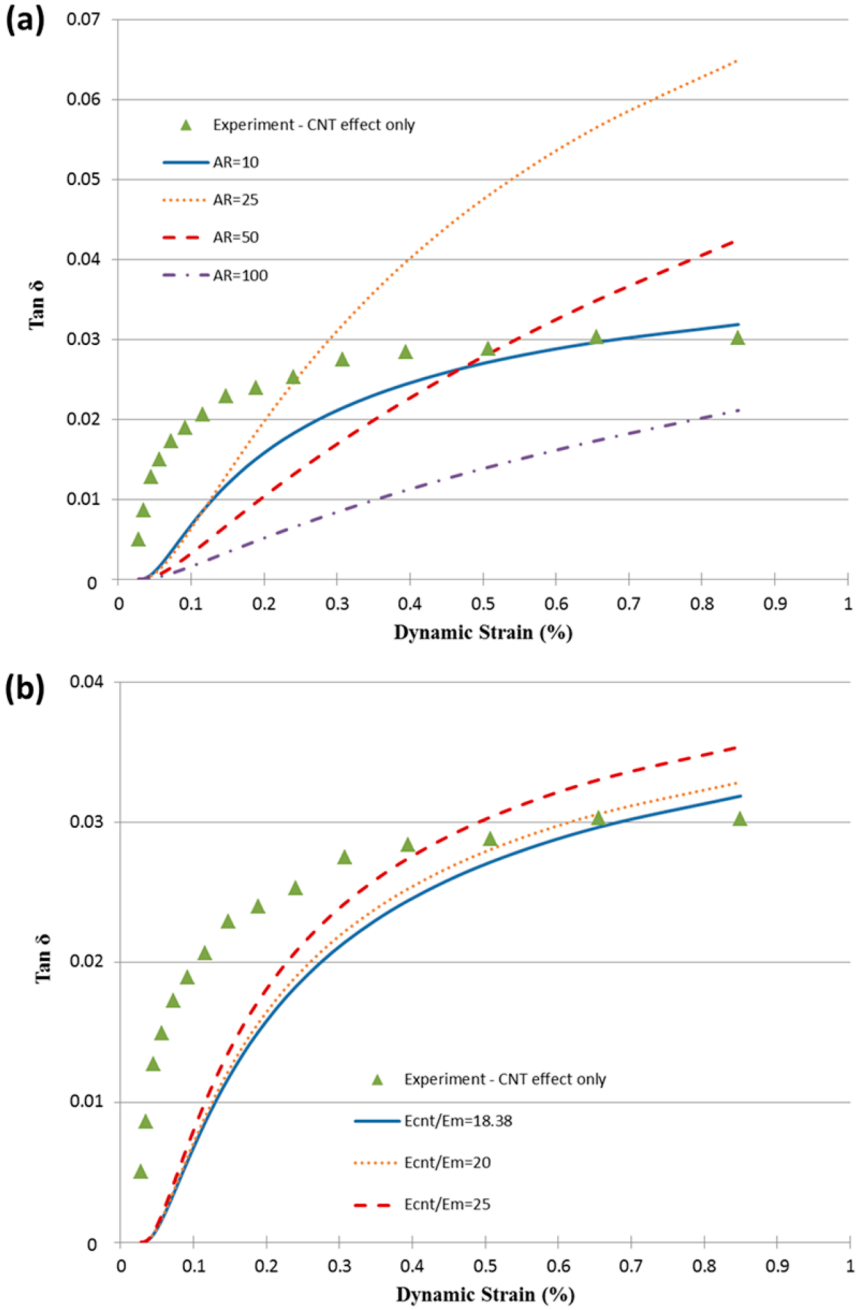


**Figure 8.** Results of tan $\delta$ as a function of dynamic strain for 1 wt % aligned CNT/PS. Experimental results (with the matrix contribution subtracted) are compared to the micromechanics model from Glaz et al.[1] (a) Parametric study on the effect of aspect ratio, AR (diameter of CNT was kept constant while the length of the CNT was varied). $E_{CNT}/E_m$ = 18.38 (the effective CNT modulus of 29.9 GPa is taken from the experimental data and the rule of mixtures. $\tau_c$ = 0.443, 0.521, 0.523, 0.523 MPa for AR of 10, 25, 50, and 100, respectively). (b) Parametric study of modulus ratio between CNT ($E_{CNT}$) and matrix ($E_m$) (AR = 10 and $\tau_c$ = 0.443, 0.454, 0.482 MPa for modulus ratios of 18.38, 20, and 25, respectively).

frequency is decreased, suggesting that polymer relaxation at the interface has reduced the interfacial shear stress, requiring higher axial strains to overcome the interfacial shear strength at the lower frequency.

Because the polystyrene chains and pristine CNTs are both unpolar, the vdW forces are expected to be mainly caused by interactions between instantaneously induced dipoles (dispersion forces). In addition, it is argued here that adhesive vdW interactions do not contribute significantly to interfacial shear interactions, because they depend on fluctuations in charge distribution,[32] which occurs at much higher frequencies than those studied here. Moreover, some of the relaxation modes of polymer chains are active in the explored range of frequency.[33] These relaxation modes facilitate the reconfiguration of polymer chains around the CNT reinforcements and conformal to CNT surface roughness, suppressing the stresses accumulated in the polymer because of mechanical interlocking during sliding. A clear indication of the active relaxation modes within the polymer at the studied frequencies is the reduction in composite storage modulus by ~3% at 0.1 Hz compared to the 1.0 Hz storage modulus. Therefore, these results indicate that the mechanical interlocking is the dominant strain energy dissipation mechanism for the nanocomposite system studied here. This is in contrast to previous studies, for example,[13] in


DOI: 10.1021/acsami.5b01459
ACS Appl. Mater. Interfaces 2015, 7, 9725−9735

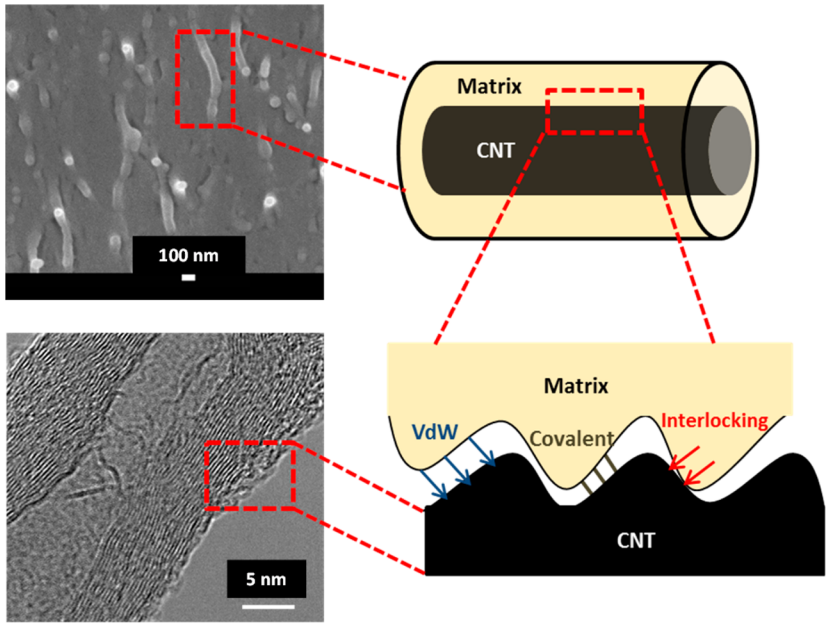


**Figure 9.** Schematic of interfacial interactions between a CNT and polymer in a CNT/polymer composite inspired by the SEM image of the composite and the TEM image showing the surface topography of the CNT.

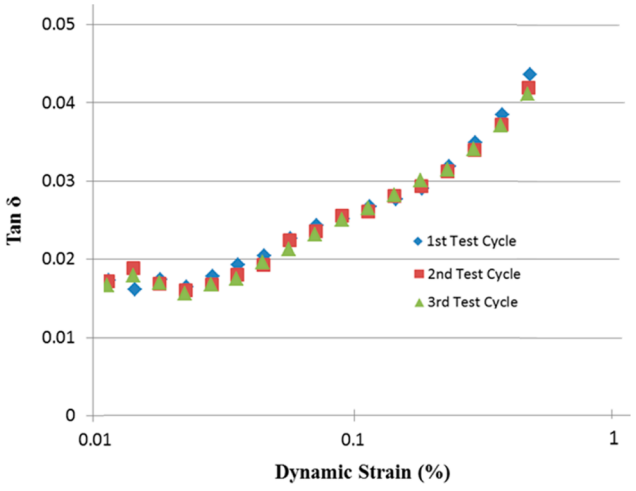


**Figure 10.** Experimental results of tan $\delta$ as a function of dynamic strain for a 1 wt % aligned CNT/PS sample. Multiple tests cycles were performed on the same sample.

which vdW forces have been postulated but not quantitatively substantiated as the dominant interfacial slip mechanism. In addition, the slope of the tan $\delta$ vs dynamic strain data for 1 and 0.1 Hz, shown in Figure 11a, shows an increase with an increase in frequency. This result shows that not only does the onset of slippage occur earlier for higher frequency but also that debonding occurs at a larger rate. That is, for a given strain, the length over which slip occurs is larger for the higher frequency case, as verified by observation of eqs 9 and 10. This justifies the claim that lower frequency leads to suppression of stress accumulation at the interface, postponing interfacial failure.

## 5. CONCLUSIONS

Damping in nanocomposites is investigated with a focus on the interfacial phenomena resulting from the presence of the CNT fillers in the polymer matrix. The CNTs were dominantly oriented parallel to the loading direction to minimize the

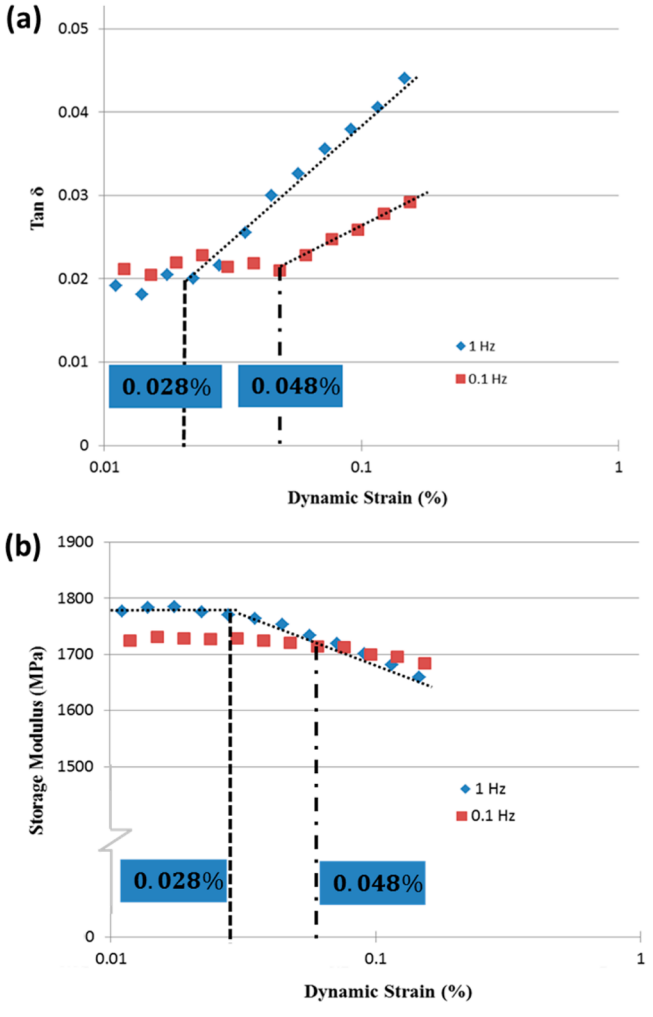


**Figure 11.** Experimental results of (a) tan $\delta$ and (b) storage modulus as a function of dynamic strain 1 wt % aligned CNT/PS composite at frequencies of 0.1 and 1 Hz. Offset strain = 0.0%.



DOI: 10.1021/acsami.5b01459
ACS Appl. Mater. Interfaces 2015, 7, 9725−9735

contribution of damping mechanisms other than inherent damping of matrix and interfacial slip, in contrast to randomly oriented CNTs where other energy dissipation mechanisms, such as matrix tearing and plasticity, can also be active. The role of fiber−matrix interactions was studied, pointing to a "slip-stick" mechanism as the source for energy dissipation. Our results point to the major contribution of mechanical interlocking, after the initiation of interfacial slip, to energy dissipation in the composite. Moreover, interfacial slippage between pristine CNTs and PS was measured to occur at strains as low as 0.028%, mainly because of shear stress concentration along the interface and weak interfaces, caused by the elastic mismatch between CNTs and polymer. After the initial interface failure, the frictional sliding at the interface increased the energy dissipation by as much as 100% compared to the inherent damping capability of the matrix, depending on the magnitude of the dynamic strain amplitude. The use of CNT interfacial slip as a damping mechanism in polymer composites has the potential for damping augmentation in rotary-wing structures and enhancement of aerodynamic stability applications. More specifically, the repeatability of the damping properties during multiple cycles of loading without accumulation of damage at the interface shows promise in aerodynamic applications where energy dissipation capability is vital to the performance of the structure throughout its life cycle.

## APPENDIX

The storage modulus of the CNT was calculated using a rule of mixtures approach with input from the experimental results, Figure 5, at the lowest tested strain. It was assumed that the load was carried only by the outmost shell. The composite modulus, $E_c$ = 1781 MPa, and the neat polymer modulus, $E_m$ = 1630 MPa, were taken from an average value of the modulus at the lowest strains tested (below the critical dynamic strain). The volume fraction, $v_f$, was calculated using eq 12 for a weight fraction, $w_f$, of 0.01 and a CNT and polymer density of 2.1 and 1.04 g/cm$^3$, respectively.

$$v_f = \frac{w_f \rho_m}{w_f \rho_m + (1 - w_f)\rho_{CNT}} \tag{12}$$

In reality the CNTs are hollow and the outer shell carries the majority of the load. The modulus of the CNT, $E_{shellCNT}$, was calculated using eq 13, assuming highly aligned, cylindrical inclusions.

$$E_c = (1 - v_f)E_m + v_f E_{shellCNT}\frac{4t}{d} \tag{13}$$

The thickness of the outer shell, $t$, was assumed to be 0.34 nm and the diameter of the CNTs, $d$, to be in the range of 30−50 nm. This leads to a CNT modulus range of 702 GPa < $E_{shellCNT}$ < 1.17 TPa. This range of values of CNT shell stiffness is comparable to measured/predicted modulus of CNT shells.[34]

## AUTHOR INFORMATION

### Corresponding Author

*E-mail: naraghi@aero.tamu.edu. Tel.: (979) 862-3323. Fax: 979-845-6051. Webpage: http://aero.tamu.edu/faculty/naraghi.

### Notes

The authors declare no competing financial interest.

## ACKNOWLEDGMENTS

Use of the TAMU Materials Characterization Facility is acknowledged. M.N. and D.C.L. would like to acknowledge the support of DOD − Army Research Laboratory, under the award No. W911NF-14-2-0080.

## REFERENCES

(1) Glaz, B.; Riddick, J.; Habtour, E.; Kang, H. Interfacial Strain Energy Dissipation in Hybrid Nanocomposite Beams under Axial Strain Fields. *AIAA J.* **2015**, DOI: 10.2514/2511.J053390.

(2) Chen, V. C. Analysis of Radar Micro-Doppler with Time-Frequency Transform. In *Proceedings of Tenth IEEE Workshop on the Statistical Signal and Array Processing*; IEEE: Piscataway, NJ, 2000; pp 463−466.

(3) Aiken, E. W.; Ormiston, R. A.; Young, L. A. Future Directions in Rotorcraft Technology at Ames Research Center. In *Proceedings of the 56th American Helicopter Society Annual Forum*; Virginia Beach, VA, May 1−22, 2000 ; American Helicopter Society International: Fairfax, VA, 2000; pp 1−22.

(4) Finegan, I. C.; Gibson, R. F. Recent Research on Enhancement of Damping in Polymer Composites. *Compos. Struct.* **1999**, *44*, 89−98.

(5) Gangopadhyay, R.; De, A. Conducting Polymer Nanocomposites: A Brief Overview. *Chem. Mater.* **2000**, *12*, 608−622.

(6) Harris, P. Carbon Nanotube Composites. *Int. Mater. Rev.* **2004**, *49*, 31−43.

(7) Schmitt, C.; Lebienvenu, M. Electrostatic Painting of Conductive Composite Materials. *J. Mater. Process. Technol.* **2003**, *134*, 303−309.

(8) Chen, C.; Lakes, R. Analysis of High-Loss Viscoelastic Composites. *J. Mater. Sci.* **1993**, *28*, 4299−4304.

(9) Gong, Z.; Gong, J.; Yan, X.; Gao, S.; Wang, B. Investigation of the Effects of Temperature and Strain on the Damping Properties of Polycarbonate/Multiwalled Carbon Nanotube Composites. *J. Phys. Chem. C* **2011**, *115*, 18468−18472.

(10) Tserpes, K. I.; Papanikos, P. Finite Element Modeling of Single-Walled Carbon Nanotubes. *Composites Part B* **2005**, *36*, 468−477.

(11) Lau, K.-T.; Chipara, M.; Ling, H.-Y.; Hui, D. On the Effective Elastic Moduli of Carbon Nanotubes for Nanocomposite Structures. *Composites, Part B* **2004**, *35*, 95−101.

(12) Naraghi, M.; Chawla, S. Carbonized Micro-and Nanostructures: Can Downsizing Really Help? *Materials* **2014**, *7*, 3820−3833.

(13) Suhr, J.; Koratkar, N. A. Energy Dissipation in Carbon Nanotube Composites: A Review. *J. Mater. Sci.* **2008**, *43*, 4370−4382.

(14) Ogasawara, T.; Tsuda, T.; Takeda, N. Stress−Strain Behavior of Multi-Walled Carbon Nanotube/Peek Composites. *Compos. Sci. Technol.* **2011**, *71*, 73−78.

(15) Cox, H. The Elasticity and Strength of Paper and Other Fibrous Materials. *Br. J. Appl. Phys.* **1952**, *3*, 72.

(16) Ang, K. K.; Ahmed, K. S. An Improved Shear-Lag Model for Carbon Nanotube Reinforced Polymer Composites. *Composites, Part B* **2013**, *50*, 7−14.

(17) Esteva, M.; Spanos, P. Effective Elastic Properties of Nanotube Reinforced Composites with Slightly Weakened Interfaces. *J. Mech. Mater. Struct.* **2009**, *4*, 887−900.

(18) Desai, A.; Haque, M. Mechanics of the Interface for Carbon Nanotube−Polymer Composites. *Thin-walled structures* **2005**, *43*, 1787−1803.

(19) Chandra, R.; Singh, S.; Gupta, K. Damping Studies in Fiber-Reinforced Composites−a Review. *Compos. Struct.* **1999**, *46*, 41−51.

(20) Liew, K.; He, X.; Wong, C. On the Study of Elastic and Plastic Properties of Multi-Walled Carbon Nanotubes under Axial Tension Using Molecular Dynamics Simulation. *Acta Mater.* **2004**, *52*, 2521−2527.

(21) Rao, A.; Jorio, A.; Pimenta, M.; Dantas, M.; Saito, R.; Dresselhaus, G.; Dresselhaus, M. Polarized Raman Study of Aligned Multiwalled Carbon Nanotubes. *Phys. Rev. Lett.* **2000**, *84*, 1820.

(22) Brown, S.; Jorio, A.; Dresselhaus, M.; Dresselhaus, G. Observations of the D-Band Feature in the Raman Spectra of Carbon Nanotubes. *Phys. Rev. B* **2001**, *64*, 073403.



DOI: 10.1021/acsami.5b01459
*ACS Appl. Mater. Interfaces* 2015, 7, 9725−9735

(23) Hwang, S.; Gibson, R. Micromechanical Modeling of Damping in Discontinuous Fiber Composites Using a Strain Energy/Finite Element Approach. *J. Eng. Mater. Technol.* **1987**, *109*, 47−52.
(24) Li, C.; Chou, T.-W. Multiscale Modeling of Carbon Nanotube Reinforced Polymer Composites. *J. Nanosci. Nanotechnol.* **2003**, *3*, 423−430.
(25) Gao, X.-L.; Li, K. A Shear-Lag Model for Carbon Nanotube-Reinforced Polymer Composites. *Int. J. Solids Struct.* **2005**, *42*, 1649−1667.
(26) Gibson, R.; Chaturvedi, S.; Sun, C. Complex Moduli of Aligned Discontinuous Fibre-Reinforced Polymer Composites. *J. Mater. Sci.* **1982**, *17*, 3499−3509.
(27) Suarez, S.; Gibson, R.; Sun, C.; Chaturvedi, S. The Influence of Fiber Length and Fiber Orientation on Damping and Stiffness of Polymer Composite Materials. *Exp. Mech.* **1986**, *26*, 175−184.
(28) Suhr, J.; Koratkar, N.; Keblinski, P.; Ajayan, P. Viscoelasticity in Carbon Nanotube Composites. *Nat. Mater.* **2005**, *4*, 134−137.
(29) Schadler, L.; Giannaris, S.; Ajayan, P. Load Transfer in Carbon Nanotube Epoxy Composites. *Appl. Phys. Lett.* **1998**, *73*, 3842−3844.
(30) Liao, K.; Li, S. Interfacial Characteristics of a Carbon Nanotube−Polystyrene Composite System. *Appl. Phys. Lett.* **2001**, *79*, 4225−4227.
(31) Wong, M.; Paramsothy, M.; Xu, X.; Ren, Y.; Li, S.; Liao, K. Physical Interactions at Carbon Nanotube-Polymer Interface. *Polymer* **2003**, *44*, 7757−7764.
(32) Parsegian, V. A. Van Der Waals Forces: A Handbook for Biologists, Chemists, Engineers, and Physicists. *Phys. Rev. Lett.* **2013**, *82*, 5397.
(33) Holmes, L. A.; Kusamizu, S.; Osaki, K.; Ferry, J. D. Dynamic Mechanical Properties of Moderately Concentrated Polystyrene Solutions. *J. Polym. Sci., Part A-2: Polym. Phys.* **1971**, *9*, 2009−2021.
(34) Coleman, J. N.; Khan, U.; Blau, W. J.; Gun'ko, Y. K. Small but Strong: A Review of the Mechanical Properties of Carbon Nanotube−Polymer Composites. *Carbon* **2006**, *44*, 1624−1652.


DOI: 10.1021/acsami.5b01459
*ACS Appl. Mater. Interfaces* 2015, 7, 9725−9735